An Upwind Differencing Scheme For The Time-Accurate Incompressible Navier-Stokes Equations

Stuart E. Rogers and Dochan Kwak
NASA Ames Research Center, MS T047-1, Moffett Field, CA 94035-1000

Originally appeared as AIAA Paper 88-2583, June 1988.
Published in *AIAA Journal*, Vol. 28, No. 2, February, 1990, pp. 253–262.

Abstract

The two-dimensional incompressible Navier-Stokes equations are solved in a time-accurate manner using the method of pseudocompressibility. Using this method, subiterations in pseudo-time are required to satisfy the continuity equation at each time step. An upwind differencing scheme based on flux-difference splitting is used to compute the convective terms. The upwind differencing is biased based on the sign of the local eigenvalue of the Jacobian matrix of the convective fluxes. Both third-order and fifth-order differencing schemes are used on the convective fluxes throughout the grid's interior. The equations are solved using an implicit line relaxation scheme. This solution scheme is stable and is capable of running at large time steps in pseudo-time, leading to fast convergence for each physical time step. A variety of computed results are presented to validate the present scheme. Results for the flow over an oscillating plate are compared with the exact analytic solution, good agreement is seen. Excellent comparison is obtained between the computed solution and the analytical results for inviscid channel flow with an oscillating back pressure. Flow solutions over a circular cylinder with vortex shedding are also presented. Finally, the flow past an airfoil at -90° angle of attack is also computed.

Introduction

Time-accurate solutions to the incompressible Navier-Stokes equations are currently of interest in the field of computational fluid dynamics (CFD). The primary problem in obtaining time-accurate solutions to the incompressible Navier-Stokes equations involves the difficulties of coupling changes in the velocity field with changes in the pressure field while satisfying the continuity equation. Since the equations are elliptic in nature, they require that all disturbances propagate to all points in the flow field in a single time step. Thus some type of iterative scheme is usually required to solve the equations in time. The stream-function vorticity formulation of the equations has been used often when only two-dimensional (2-D) problems are of interest, but this has no straight forward extension to three-dimensions (3-D). As the goal of the current work involves developing a solution methodology which can be used to compute complex unsteady 3-D incompressible flows, this paper will be limited to a discussion of methods using primitive variables.

Most methods using primitive variables can be classified into three groups. The first of these, and historically one of the most commonly used primitive variable schemes, is the pressure Poisson method as first introduced by Harlow and Welch.[1] In this method, the velocity field is advanced in time using the momentum equations. Then a Poisson equation in pressure, which is formed from the momentum equations, is solved for the pressure at the current time level such that the continuity equation will be satisfied at the next time level. In this method the velocity and pressure are indirectly coupled. The second group of methods can be classified as fractional step methods. This idea was first introduced by Chorin,[2] and is characterized by first solving for an intermediate velocity from the momentum equations, and then solving for a pressure field which will map the intermediate velocity into a divergent-free velocity. Computing the pressure field usually is usually accomplished by solving a Poisson equation in pressure, which can be very costly.

The third method is that of artificial compressibility. This method was first introduced by Chorin[3] for use in obtaining steady-state solutions to the incompressible Naiver-Stokes equations, and has been used with much success by many authors, see for example Kwak *et al.*[4] Several authors have recently used this method successfully in computing time-accurate problems. Merkle and Athavale[5] presented solutions using this approach in 2-D generalized coordinates. Soh and Goodrich[6] also present solutions for a Cartesian mesh in 2-D. In the artificial compressibility formulation, a pseudo-time derivative of pressure is added to the continuity equation which directly couples the pressure and velocity. The equations are advanced in physical time by iterating until a divergent-free velocity field is obtained at the new physical time level. Similarities exist

between this formulation and the fractional step method of Chorin[2] because his mapping of the intermediate velocity field to a divergent-free velocity field is based on the artificial compressibility approach. However, the artificial compressibility method is different in that it affords a direct coupling between the pressure and velocity as they are advanced in time.

The goal of the current work is to develop a method to solve the incompressible Navier-Stokes equations in a time-accurate and efficient manner so it can be used in solving complex 3-D problems in generalized coordinates which may require a large number (100,000 to 500,000) of grid points. In an effort to do this, the 2-D Navier-Stokes equations in generalized coordinates are studied to obtain a method which can be extended to the desired goal of a 3-D flow solver. The recent work toward this goal uses an artificial compressibility approach to solve the incompressible Navier-Stokes equations in a time-accurate manner. This method was used to take advantage of some recent advances in the artificial compressibility formulation, namely the use of flux-difference splitting to upwind-difference the convective terms as developed by Rogers and Kwak,[7] and Hartwich and Hsu.[8] A line-relaxation scheme is used to solve the equations, which will provide the stability to converge pseudo-time iterations rapidly. This will also help to ensure that the physical time-step size will be bounded by the physical constraints of the problem and not by the numerical stability.

In the following sections, details of the artificial compressibility scheme are given. Once these equations have been established, the details of their numerical solution are discussed, including the use of flux-difference splitting to compute the convective terms, and the line relaxation used to solve the equations in pseudo-time. The computed results section presents results for the flow over an oscillating plate, the flow through an inviscid channel with a time-varying back pressure, the flow over a circular cylinder, and the flow over an airfoil at -90° angle of attack. This last problem is motivated by the study of the downloads on the wing of the XV-15 Tilt Rotor aircraft in hover.

Governing Equations

The governing equations for incompressible, constant density flow are written in conservative form with the density absorbed by the pressure term. Generalized coordinates are used of the form

$$\begin{aligned} \xi &= \xi(x, y, t) \\ \eta &= \eta(x, y, t) \end{aligned} \tag{1}$$

resulting in the following system of equations

$$\begin{aligned} \frac{\partial \hat{u}}{\partial t} &= -\frac{\partial}{\partial \xi}(\hat{e} - \hat{e}_v) - \frac{\partial}{\partial \eta}(\hat{f} - \hat{f}_v) = -\hat{r} \\ \frac{\partial}{\partial \xi}\left(\frac{U}{J}\right) &+ \frac{\partial}{\partial \eta}\left(\frac{V}{J}\right) = 0 \end{aligned} \tag{2a}$$

where $\hat{r}$ represents the right-hand side of the momentum equations, where J is the Jacobian of

the transformation and

$$\begin{aligned}
\hat{u} &= \frac{1}{J}\begin{bmatrix} u \\ v \end{bmatrix} \\
\hat{e} &= \frac{1}{J}\begin{bmatrix} \xi_x p + uU + \xi_t u \\ \xi_y p + vU + \xi_t v \end{bmatrix} \\
\hat{f} &= \frac{1}{J}\begin{bmatrix} \eta_x p + uV + \eta_t u \\ \eta_y p + vV + \eta_t v \end{bmatrix} \\
U &= \xi_x u + \xi_y v \\
V &= \eta_x u + \eta_y v
\end{aligned} \tag{2b}$$

In deriving the viscous fluxes, constant viscosity was assumed for simplicity and because initially only laminar flow calculations are being performed. This simplification is not necessary and will be removed in the future. The viscous fluxes are then given by

$$\begin{aligned}
\hat{e}_v &= \frac{\nu}{J}\begin{bmatrix} (\xi_x^2 + \xi_y^2)u_\xi + (\xi_x\eta_x + \xi_y\eta_y)u_\eta \\ (\xi_x^2 + \xi_y^2)v_\xi + (\xi_x\eta_x + \xi_y\eta_y)v_\eta \end{bmatrix} \\
\hat{f}_v &= \frac{\nu}{J}\begin{bmatrix} (\xi_x\eta_x + \xi_y\eta_y)u_\xi + (\eta_x^2 + \eta_y^2)u_\eta \\ (\xi_x\eta_x + \xi_y\eta_y)v_\xi + (\eta_x^2 + \eta_y^2)v_\eta \end{bmatrix}
\end{aligned} \tag{2c}$$

where ν is the kinematic viscosity. If an orthgonal grid is assumed then the viscous fluxes reduce to

$$\begin{aligned}
\hat{e}_v &= \frac{\nu}{J}\begin{bmatrix} (\xi_x^2 + \xi_y^2)u_\xi \\ (\xi_x^2 + \xi_y^2)v_\xi \end{bmatrix} \\
\hat{f}_v &= \frac{\nu}{J}\begin{bmatrix} (\eta_x^2 + \eta_y^2)u_\eta \\ (\eta_x^2 + \eta_y^2)v_\eta \end{bmatrix}
\end{aligned} \tag{2d}$$

In the preceding equations, the metrics of the transformation have been represented by

$$\frac{\partial \xi}{\partial x} = \xi_x, \text{ etc.}$$

and the velocity gradients in the viscous fluxes were written as

$$\frac{\partial u}{\partial \xi} = u_\xi, \text{ etc.}$$

The time derivatives in the momentum equations are differenced using a second-order three-point implicit formula

$$\frac{1.5\hat{u}^{n+1} - 2\hat{u}^n + 0.5\hat{u}^{n-1}}{\Delta t} = -\hat{r}^{n+1} \tag{3}$$

where the superscript n denotes the quantities at time $t = n\Delta t$ and $\hat{r}$ is the residual given in Eq. (2a). To solve Eq. (3) for a divergence free velocity at the *n+1* time level, a pseudo-time level is introduced and is denoted by a superscript m. The equations are iteratively solved such that $\hat{u}^{n+1,m+1}$ approaches the new velocity $\hat{u}^{n+1}$ as the divergence of $\hat{u}^{n+1,m+1}$ approaches zero. To drive the divergence of this velocity to zero, the following artificial compressibility relation is introduced:

$$\frac{\partial p}{\partial \tau} = -\beta \nabla \cdot \hat{u}^{n+1,m+1} \tag{4}$$

where τ denotes pseudo-time and where β is an artificial compressibility parameter. Applying an implicit Euler time differencing to Eq. (4) and rewriting Eq. (3) with the pseudo-time superscripts gives

$$\begin{aligned}
&\frac{\hat{p}^{n+1,m+1} - \hat{p}^{n+1,m}}{\Delta\tau} = -\beta \left[\frac{\partial}{\partial\xi}\left(\frac{U}{J}\right) + \frac{\partial}{\partial\eta}\left(\frac{V}{J}\right) \right]^{n+1,m+1} \\
&\frac{1.5\hat{u}^{n+1,m+1} - 1.5\hat{u}^{n+1,m}}{\Delta t} = \\
&\qquad - \hat{r}^{n+1,m+1} - \frac{1.5\hat{u}^{n+1,m} - 2\hat{u}^{n} + 0.5\hat{u}^{n-1}}{\Delta t}
\end{aligned} \tag{5}$$

where $\hat{p} = p/J$. In this partially discretized form of the first equation, β and $\Delta\tau$ are not independent. However, both of them are kept seperate at this point because in the final discrete form, β will be independent of $\Delta\tau$ because of a nonlinear coupling between the continuity equation and momentum equations due to the upwind differencing. This will be discussed further in the upwind-differencing section.

Combining these two equations into one system of equations in delta form gives

$$\begin{aligned}
&I_{t\tau}(\hat{D}^{n+1,m+1} - \hat{D}^{n+1,m}) \\
&= -\hat{R}^{n+1,m+1} - \frac{I_m}{\Delta t}(1.5\hat{D}^{n+1,m} - 2\hat{D}^{n} + 0.5\hat{D}^{n-1})
\end{aligned} \tag{6}$$

where

$$\begin{aligned}
\hat{D} &= \frac{1}{J}\begin{bmatrix} p \\ u \\ v \end{bmatrix}; \quad D = J\hat{D} \\
\hat{R} &= \frac{\partial}{\partial\xi}(\hat{E} - \hat{E}_v) + \frac{\partial}{\partial\eta}(\hat{F} - \hat{F}_v) \\
\hat{E} &= \frac{1}{J}\begin{bmatrix} \beta U \\ \xi_x p + uU + \xi_t u \\ \xi_y p + vU + \xi_t v \end{bmatrix} \\
\hat{F} &= \frac{1}{J}\begin{bmatrix} \beta V \\ \eta_x p + uV + \eta_t u \\ \eta_y p + vV + \eta_t v \end{bmatrix} \\
\hat{E}_v &= \frac{\nu}{J}\begin{bmatrix} 0 \\ \hat{e}_v \end{bmatrix} \\
\hat{F}_v &= \frac{\nu}{J}\begin{bmatrix} 0 \\ \hat{f}_v \end{bmatrix}
\end{aligned}$$

and where $I_{t\tau}$ is a diagonal matrix and I_m is a modified identity matrix given by

$$\begin{aligned}
I_{t\tau} &= \text{diag}\left[\frac{1}{\Delta\tau},\ \frac{1.5}{\Delta t},\ \frac{1.5}{\Delta t}\right] \\
I_m &= \text{diag}[0,\ 1,\ 1]
\end{aligned}$$

Finally, the residual term at the *m+1* pseudo-time level is linearized giving the following equation

in delta form

$$\left[\frac{I_{t\tau}}{J^{n+1}} + \left(\frac{\partial \hat{R}}{\partial D}\right)^{n+1,m}\right](D^{n+1,m+1} - D^{n+1,m}) \\ = -\hat{R}^{n+1,m} - \frac{I_m}{\Delta t}(1.5\hat{D}^{n+1,m} - 2\hat{D}^n + 0.5\hat{D}^{n-1}) \tag{7}$$

It is noted that the flux vectors $\hat{E}_i$ are the same as would be obtained from a steady-state formulation of the artificial compressibility method except for the presence of the time-varying metric terms, which will only be non-zero for a mesh which changes with time. Therefore any differencing method which works well for the steady-state formulation will be appropriate for the current application. Although the use of upwind schemes based on flux-difference splitting is more expensive than the use of central differencing, the upwind schemes have the advantage that they add dissipation to the system naturally, whereas the central differencing requires the use of artificial dissipation. For this reason the current work uses a flux-difference splitting scheme for the spatial discretization of the convective terms in Eq. (7).

The eigensystem of the Jacobian matrix of the flux vectors is required for the formation of the upwind differencing numerical fluxes, and so the 2-D eigensystem is presented here for the current formulation. For the 3-D equations, see Rogers *et al.*,[9] or Hartwich and Hsu.[8] It should be noted that the transformation given by the latter can become singular for certain values of the metrics.

The generalized flux vector for the 2-D system of equations is given by

$$\hat{E}_i = \begin{bmatrix} \beta Q \\ k_x p + uQ + k_t u \\ k_y p + vQ + k_t v \end{bmatrix} \tag{8}$$

where $\hat{E}_i = \hat{E}, \hat{F}$ for $i = 1,2$ respectively, and the normalized metrics are represented with

$$k_x = \frac{1}{J}\frac{\partial \xi_i}{\partial x}, i = 1,2$$

$$k_y = \frac{1}{J}\frac{\partial \xi_i}{\partial y}, i = 1,2$$

and the scaled contravariant velocity is

$$Q = k_x u + k_y v$$

The Jacobian matrices for this system are given by

$$\hat{A}_i = \frac{\partial \hat{E}_i}{\partial D} = \begin{bmatrix} 0 & \beta k_x & \beta k_y \\ k_x & k_x u + Q + k_t & k_y u \\ k_y & k_x v & k_y v + Q + k_t \end{bmatrix} \tag{9}$$

A similarity transform for the Jacobian matrix is introduced

$$\hat{A}_i = X_i \Lambda_i X_i^{-1}$$

where

$$\begin{aligned}\Lambda_i &= \mathrm{diag}[\lambda_1, \lambda_2, \lambda_3] \\ \lambda_1 &= Q + k_t \\ \lambda_2 &= Q + c + \frac{1}{2}k_t \\ \lambda_3 &= Q - c + \frac{1}{2}k_t\end{aligned} \tag{10}$$

and where c is the scaled artificial speed of sound given by

$$c = \sqrt{(Q + \frac{1}{2}k_t)^2 + \beta(k_x^2 + k_y^2)} \tag{11}$$

The matrix of the right eigenvectors is given by

$$X_i = \frac{1}{2\beta c(c^2 - \frac{1}{4}k_t^2)} \begin{bmatrix} 0 & \beta(c^2 - \frac{1}{4}k_t^2) & -\beta(c^2 - \frac{1}{4}k_t^2) \\ -2\beta c k_y & (u\lambda_2 + \beta k_x)(c + \frac{1}{2}k_t) & (u\lambda_3 + \beta k_x)(c - \frac{1}{2}k_t) \\ 2\beta c k_x & (v\lambda_2 + \beta k_y)(c + \frac{1}{2}k_t) & (v\lambda_3 + \beta k_y)(c - \frac{1}{2}k_t) \end{bmatrix} \tag{12}$$

and its inverse is given by

$$X_i^{-1} = \begin{bmatrix} k_y u - k_x v & -v\lambda_1 - \beta k_y & u\lambda_1 + \beta k_x \\ -\lambda_3 & \beta k_x & \beta k_y \\ -\lambda_2 & \beta k_x & \beta k_y \end{bmatrix} \tag{13}$$

Upwind Differencing

Upwind differencing is used in the present scheme as a means of following the propagation of the artificial waves introduced by the artificial compressibility. The upwind differencing thus provides a dissipative scheme which automatically suppresses any oscillations caused by the nonlinear convective fluxes. In addition, the upwind-differenced flux vector will contribute to terms on the main diagonal of the Jacobian of the residual, whereas a central-differenced flux vector would not. This will help to make the implicit scheme nearly diagonally dominant and contribute greatly to the robustness of the code. Even though the upwind flux differences are more costly to form, the speed up in convergence could result in a significant savings in computing-time requirements.

The flux-difference split form of upwind differencing used in the current work is presented for a one-dimensional (1-D) system. In its application to multi-dimensional problems, it is applied to each coordinate direction separately. The 1-D representation of a hyperbolic system of equations in conservation law form is given by

$$\frac{\partial q}{\partial t} + \frac{\partial f}{\partial x} = 0 \tag{14}$$

where q is the vector of dependent variables and f is the flux vector. A semi-discrete approximation to this equation is given by

$$\left(\frac{\partial q}{\partial t}\right)_j + \frac{[\tilde{f}_{j+1/2} - \tilde{f}_{j-1/2}]}{\Delta x} = 0 \tag{15}$$

where $\tilde{f}$ is a numerical flux and j is a spatial index.

A flux resulting in a first-order scheme is defined by

$$\tilde{f}_{j+1/2} = \frac{1}{2}[f(q_{j+1}) + f(q_j)] - \frac{1}{2}\left[\Delta f^+_{j+1/2} - \Delta f^-_{j+1/2}\right] \tag{16}$$

where $\Delta f^{\pm}$ is the flux difference across positive or negative traveling waves. The flux difference is taken as

$$\Delta f^{\pm}_{j+1/2} = A^{\pm}(\bar{q})\Delta q_{j+1/2} \tag{17}$$

where A represents the Jacobian matrix $\partial f/\partial q$. The A^+ and A^- matrices are computed first by forming a diagonal matrix of the positive eigenvalues, and multiplying through by the similarity transform, and since the A^+ matrix plus the A^- matrix equals the original Jacobian matrix, we have

$$\begin{aligned} A^+ &= X\Lambda^+X^{-1} \\ A^- &= A - A^+ \end{aligned} \tag{18}$$

where X is the matrix of right eigenvectors of A, X^{-1} is it's inverse. The flux difference is evaluated at the mid-point by using the average of q:

$$\bar{q} = \frac{1}{2}(q_{j+1} + q_j)$$

The Δq term is given by

$$\Delta q_{j+1/2} = q_{j+1} - q_j$$

A scheme of arbitrary order may be derived using these flux differences. Implementation of higher-order accurate schemes on the right-hand side of the equations does not require significantly more computational time if the flux differences $\Delta f^{\pm}$ are all computed at once for a single line. A third-order upwind flux is defined by

$$\begin{aligned} \tilde{f}_{j+1/2} = &\frac{1}{2}[f(q_{j+1}) + f(q_j)] \\ &+ \frac{1}{6}[\Delta f^+_{j-1/2} - \Delta f^+_{j+1/2} + \Delta f^-_{j+1/2} - \Delta f^-_{j+3/2}] \end{aligned} \tag{19}$$

where the flux differences are the same as in the first-order difference given by Eq. (17).

The primary problem with using schemes of accuracy greater than second order occurs at the boundaries. Large stencils will require special treatment at the boundaries, and a reduction of order is necessary. Therefore, when going to a higher-order accurate scheme, compactness is desirable. Such a scheme was used by Rai[10] using a fifth-order accurate upwind-biased stencil. A fifth-order fully upwind difference would require 11 points, but this upwind-biased scheme requires only 7 points. It is given by

$$\begin{aligned} \tilde{f}_{j+1/2} = &\frac{1}{2}[f(q_{j+1}) + f(q_j)] \\ &+ \frac{1}{60}[-2\Delta f^+_{j-3/2} + 11\Delta f^+_{j-1/2} - 6\Delta f^+_{j+1/2} - 3\Delta f^+_{j+3/2}] \\ &+ \frac{1}{60}[2\Delta f^-_{j+5/2} - 11\Delta f^-_{j+3/2} + 6\Delta f^-_{j+1/2} + 3\Delta f^-_{j-1/2}] \end{aligned} \tag{20}$$

At points adjacent to the boundary, the high-order stencils cannot be maintained and the order of the scheme must be reduced. However, it is not necessary to reduce the accuracy to first-order. The following flux is used at points next to the boundary

$$\tilde{f}_{j+1/2} = \frac{1}{2}[f(q_{j+1}) + f(q_j)] - \frac{\epsilon}{2}\left[\Delta f^+_{j+1/2} - \Delta f^-_{j+1/2}\right] \tag{21}$$

For $\epsilon = 0$, this flux leads to a second-order central difference. For $\epsilon = 1$, this is the same as the first-order upwind difference given by Eq. (16). By including the delta-flux terms with a small value for the coefficient ϵ, near second-order accuracy is maintained and the added dissipation ensures that no oscillations occur at the boundary. This boundary treatment has been found to work well for very small values of ϵ. A value of 0.01 was used for all the results presented in this paper.

The right and left matrices given by equations (12,13) clearly show that the artificial compressibility parameter β will affect not only the continuity equations, but the momentum equations as well. An analysis for the cartesian coordinate case shows that the dissipation terms added to the momentum equations will grow as the square root of β. This indicates that the value of β should be chosen with care when using the upwind-differencing, as extremely large values could cause large errors in the differencing of the momentum equations.

Implicit Scheme

This section describes the way in which Eq. (7) is numerically represented and solved. The first consideration is the formation of the Jacobian matrix of the residual vector $\hat{R}$ required for the implicit side of the equation. Applying the semi-discrete formula given in Eq. (15) to the flux vectors, and applying a second-order central difference formula to the viscous terms, the residual at a discrete point $x_{i,j}, y_{i,j}$ is given by

$$\begin{aligned} R_{i,j} = &\frac{\tilde{E}_{i+1/2,j} - \tilde{E}_{i-1/2,j}}{\Delta\xi} + \frac{\tilde{F}_{i,j+1/2} - \tilde{F}_{i,j-1/2}}{\Delta\eta} \\ &- \frac{(\hat{E}_v)_{i+1,j} - (\hat{E}_v)_{i-1,j}}{2\Delta\xi} - \frac{(\hat{F}_v)_{i,j+1} - (\hat{F}_v)_{i,j-1}}{2\Delta\eta} \end{aligned} \tag{22}$$

where i and j are indices for the ξ and η directions, respectively. The generalized coordinates are chosen so that $\Delta\xi$ and $\Delta\eta$ are equal to one. Applying the first-order upwind numerical flux in Eq. (16) gives

$$\begin{aligned} R_{i,j} = &\frac{1}{2}\big[\hat{E}_{i+1,j} - \hat{E}_{i-1,j} + \hat{F}_{i,j+1} - \hat{F}_{i,j-1} \\ &- \Delta E^+_{i+1/2,j} + \Delta E^-_{i+1/2,j} + \Delta E^+_{i-1/2,j} - \Delta E^-_{i-1/2,j} \\ &- \Delta F^+_{i,j+1/2} + \Delta F^-_{i,j+1/2} + \Delta F^+_{i,j-1/2} - \Delta F^-_{i,j-1/2} \\ &- (\hat{E}_v)_{i+1,j} + (\hat{E}_v)_{i-1,j} - (\hat{F}_v)_{i,j+1} + (\hat{F}_v)_{i,j-1}\big] \end{aligned} \tag{23}$$

The Jacobian matrix of the residual vector will form a banded matrix of the form:

$$\begin{aligned} \frac{\partial R}{\partial D} = \mathcal{B}\Big[&\frac{\partial R_{i,j}}{\partial D_{i,j-1}}, 0, ..., 0, \frac{\partial R_{i,j}}{\partial D_{i-1,j}}, \frac{\partial R_{i,j}}{\partial D_{i,j}}, \\ &\frac{\partial R_{i,j}}{\partial D_{i+1,j}}, 0, ..., 0, \frac{\partial R_{i,j}}{\partial D_{i,j+1}}\Big] \end{aligned} \tag{24}$$

The exact Jacobians of the flux differences, however, can be very costly to form. Instead, approximate Jacobians of the flux differences as derived and analyzed by both Barth[11] and Yee[12] are used. These are given as follows

$$\begin{aligned}
\frac{\partial R_{i,j}}{\partial D_{i,j-1}} &\approx \frac{1}{2}(-\hat{B}_{i,j-1} - B^+_{i,j-1/2} + B^-_{i,j-1/2}) + (\gamma_2)_{i,j-1} \\
\frac{\partial R_{i,j}}{\partial D_{i-1,j}} &\approx \frac{1}{2}(-\hat{A}_{i-1,j} - A^+_{i-1/2,j} + A^-_{i-1/2,j}) + (\gamma_1)_{i-1,j} \\
\frac{\partial R_{i,j}}{\partial D_{i,j}} &\approx \frac{1}{2}(\ A^+_{i+1/2,j} + A^+_{i-1/2,j} - A^-_{i+1/2,j} - A^-_{i-1/2,j} \\
&\qquad B^+_{i,j+1/2} + B^+_{i,j-1/2} - B^-_{i,j+1/2} - B^-_{i,j-1/2}) \\
\frac{\partial R_{i,j}}{\partial D_{i+1,j}} &\approx \frac{1}{2}(\ \hat{A}_{i+1,j} - A^+_{i+1/2,j} + A^-_{i+1/2,j}) - (\gamma_1)_{i+1,j} \\
\frac{\partial R_{i,j}}{\partial D_{i,j+1}} &\approx \frac{1}{2}(\ \hat{B}_{i,j+1} - B^+_{i,j+1/2} + B^-_{i,j+1/2}) - (\gamma_2)_{i,j+1}
\end{aligned} \tag{25}$$

where only the orthogonal mesh terms are retained for the implicit viscous terms giving

$$\gamma_1 = \frac{\nu}{J}(\xi_x^2 + \xi_y^2) Im \frac{\partial}{\partial \xi}$$
$$\gamma_2 = \frac{\nu}{J}(\eta_x^2 + \eta_y^2) Im \frac{\partial}{\partial \eta}$$

where Im is a modified identity matrix with a zero in the first diagonal entry.

The matrix equation is solved using a line-relaxation method. The entire numerical matrix equation is formed from values at the previous time level. Then the domain is swept in one or both of the two coordinate directions, once forward and once backward for each sweep. At each line perpendicular to the sweep direction, a tridiagonal matrix is formed. For the points not on this line, the implicit matrices are multiplied by the latest known ΔD vector, and the resulting vector is shifted to the right-hand side of the equations.

Boundary Conditions

Implicit boundary conditions are used for all boundaries; this helps make possible the use of large time steps. At a no-slip surface, the velocity is specified to be zero, and the pressure at the boundary is obtained by specifying the pressure gradient normal to the wall to be zero. The boundary conditions used for inflow and outflow regions are based on the method of characteristics. The formulation of these boundary conditions is similar to that given by Merkle and Tsai[13], but the implementation is slightly different. The finite-speed waves which arise with the use of artificial compressibility are governed by the following

$$\frac{\partial \hat{D}}{\partial \tau} = -\frac{\partial \hat{E}}{\partial \xi} = -\frac{\partial \hat{E}}{\partial D}\frac{\partial D}{\partial \xi} = -\hat{A}\frac{\partial D}{\partial \xi} = -X\Lambda X^{-1}\frac{\partial D}{\partial \xi}$$

then

$$X^{-1}\frac{\partial \hat{D}}{\partial \tau} = -\Lambda X^{-1}\frac{\partial D}{\partial \xi} \tag{26}$$

If one were to move the X^{-1} matrix inside the spatial and time derivative, then it can be seen that this would be a system of scalar equations, each of the form of a wave equation. The sign of the eigenvalues in the Λ matrix determines the direction of travel of the wave. For each positive (negative) eigenvalue, there is a wave propagating information in the positive (negative) ξ direction. The number of positive or negative eigenvalues determines the number of characteristic waves propagating information from the interior of the computational domain to the boundary. Thus, at the boundary, we will use these characteristics which bring information from the interior as part of our boundary conditions. The rest of the information should come from outside the computational domain, and so we are free to specify some variables.

There will either be one or two characteristics traveling toward the boundary from the interior because there is always at least one positive eigenvalue and one negative eigenvalue. In order to select the proper characteristic waves, Eq. (26) is multiplied by a diagonal selection matrix L which has an entry of one in the position of the eigenvalue we wish to select, and zeros elsewhere. Thus

$$LX^{-1}\frac{\partial \hat{D}}{\partial \tau} = -L\Lambda X^{-1}\frac{\partial D}{\partial \xi} \tag{27}$$

Replacing the time derivative with an implicit Euler time step gives

$$\left(\frac{LX^{-1}}{J\Delta\tau} + L\Lambda X^{-1}\frac{\partial}{\partial \xi}\right)(D^{n+1} - D^n) = -L\Lambda X^{-1}\frac{\partial D^n}{\partial \xi} \tag{28}$$

This gives either one or two relations, depending on the number of non-zero elements in L. To complete the set of equations, some variables must be specified to be constant. Here is defined a vector Ω of the variables to be held constant, such that

$$\frac{\partial \Omega}{\partial \tau} = 0 \longrightarrow \frac{\partial \Omega}{\partial D}\frac{\partial D}{\partial \tau} = 0 \longrightarrow \frac{\partial \Omega}{\partial D}(D^{n+1} - D^n) = 0 \tag{29}$$

Combining Eqs. (28) and (29) gives

$$\left(\frac{LX^{-1}}{J\Delta\tau} + L\Lambda X^{-1}\frac{\partial}{\partial \xi} + \frac{\partial \Omega}{\partial D}\right)(D^{n+1} - D^n) = -L\Lambda X^{-1}\frac{\partial D^n}{\partial \xi} \tag{30}$$

Equation (30) can be used to update the variables implicitly at any of the inflow or outflow boundaries with the proper choice of L and Ω.

Inflow Boundary

At the inflow, there will be one characteristic wave traveling out of the computational domain since fluid is traveling into the domain. If the incoming fluid is traveling in the positive ξ direction, then

$$\begin{aligned} Q &> 0 \\ Q + c &> 0 \\ Q - c &< 0 \end{aligned}$$

This third eigenvalue will be the one we wish to select, and so L will have a one for the third diagonal entry. If the incoming fluid is traveling in the negative ξ direction, then

$$\begin{aligned} Q &< 0 \\ Q + c &> 0 \\ Q - c &< 0 \end{aligned}$$

and the second eigenvalue is the one corresponding to the wave propagation out of the computational domain, requiring a one in the second diagonal entry of L.

Two different sets of specified variables have been used successfully for inflow boundaries. One set consists of the total pressure and the cross-flow velocity. This set is useful for problems in which the inflow velocity profile is not known. For this set the Ω vector is

$$\Omega = \begin{bmatrix} p + \frac{1}{2}(u^2 + v^2) \\ 0 \\ v \end{bmatrix} ; \frac{\partial \Omega}{\partial D} = \begin{bmatrix} 1 & u & v \\ 0 & 0 & 0 \\ 0 & 0 & 1 \end{bmatrix}$$

The second possible set of specified variables consists of the velocity components. This is useful for problems in which a specific velocity profile is desired at the inflow. The Ω vector for this is

$$\Omega = \begin{bmatrix} 0 \\ u \\ v \end{bmatrix} ; \quad \frac{\partial \Omega}{\partial D} = \begin{bmatrix} 0 & 0 & 0 \\ 0 & 1 & 0 \\ 0 & 0 & 1 \end{bmatrix}$$

Outflow Boundary

At the outflow boundary there are two characteristic waves traveling out of the computational domain since fluid is also leaving the domain. If the fluid is traveling along the positive ξ direction then

$$Q > 0$$
$$Q + c > 0$$
$$Q - c < 0$$

and we require ones in the first two diagonal entries of the L matrix. If the fluid is traveling in the negative ξ direction then

$$Q < 0$$
$$Q + c > 0$$
$$Q - c < 0$$

and we require ones in the first and third diagonal entries of the L matrix.

For all of the test problems presented in this paper static pressure was specified at the outflow boundary, resulting in

$$\Omega = \begin{bmatrix} p \\ 0 \\ 0 \end{bmatrix} ; \quad \frac{\partial \Omega}{\partial D} = \begin{bmatrix} 1 & 0 & 0 \\ 0 & 0 & 0 \\ 0 & 0 & 0 \end{bmatrix}$$

Computed Results

This section describes some computational results from the current method for several test problems. The purpose of these problems is to verify the time accuracy of the method and determine the pseudo-time convergence capability of the code. In choosing the value for β, numerical tests were done to determine a value of β resulting in the best convergence. The choice of the pseudo-time step $\Delta\tau$ was taken to be very large for all cases. This effectively reduced the

$1/\Delta\tau$ term in the diagonal matrix in Eq. (7) to zero. However, since the upwind differencing will result in terms on the diagonal in the Jacobian of the residual vector, the system will not become singular. In all cases, the time quantities given below refer to dimensionless time.

All cases were run on a Cray 2 computer, which for the present code runs at very nearly the same speed as a Cray XMP-48. The computer time required to run this code averaged $50\text{x}10^{-6}$ seconds per grid point per sub-iteration. For the problems run here, on the order of 10 subiterations are required per time-step. This leads to a computing time of on the order of $5\text{x}10^{-4}$ sec/grid point/physical time step.

Oscillating Plate

As an initial test case, the flow on top of an oscillating plate was calculated. This problem, also known as Stoke's second problem (see for example White[14]), was set up with the x-axis along the plate, and the y-axis normal to it. The velocity of the plate is set to

$$u_{plate} = u_0 \cos\omega t$$

The exact solution for this problem is given by

$$u(y,t) = u_0 \exp\left(-y\sqrt{\frac{\omega}{2\nu}}\right) \cos\left(\omega t - y\sqrt{\frac{\omega}{2\nu}}\right)$$

This is a 1-D problem in that there are no gradients in the direction parallel to the plate and so only η gradient terms were used. The mesh extended to a height where the exact solution for the velocity is less than $5\text{x}10^{-4}u_0$ and consisted of 50 points in the y-direction stretched such that the spacing at the plate was 0.002 of the total height. The velocity u_0 was set to unity, the frequency was set to 2π, and the square root term was set to unity. Thus

$$\sqrt{\frac{\omega}{2\nu}} = 1 \longrightarrow \nu = \pi$$

The physical time step Δt was set to 0.01, the pseudo-time step $\Delta\tau$ was set to 10^{12}. Since the vertical velocity component v is always zero, and there are no gradients in the x-direction, the divergence of velocity is always zero, and thus only one iteration is required to advance the equations one step in time. In fact, after one iteration, the maximum value of the right-hand side of Eq. (7) was reduced to 10^{-10}.

The problem was run over nine full periods after which time the transient solution had died off and the solution was fully periodic in time. In Fig. 1 velocity profiles at different times during the cycle are plotted for both the computed solution and the exact analytical solution. The computed solution is designated by the solid lines and the exact solution by the symbols. The $\bigcirc$ corresponds to a time of 8.25, the $\triangle$ corresponds to a time of 8.5, the + corresponds to a time of 8.75, and the $\times$ corresponds to a time of 9. Excellent comparison is seen between the two.

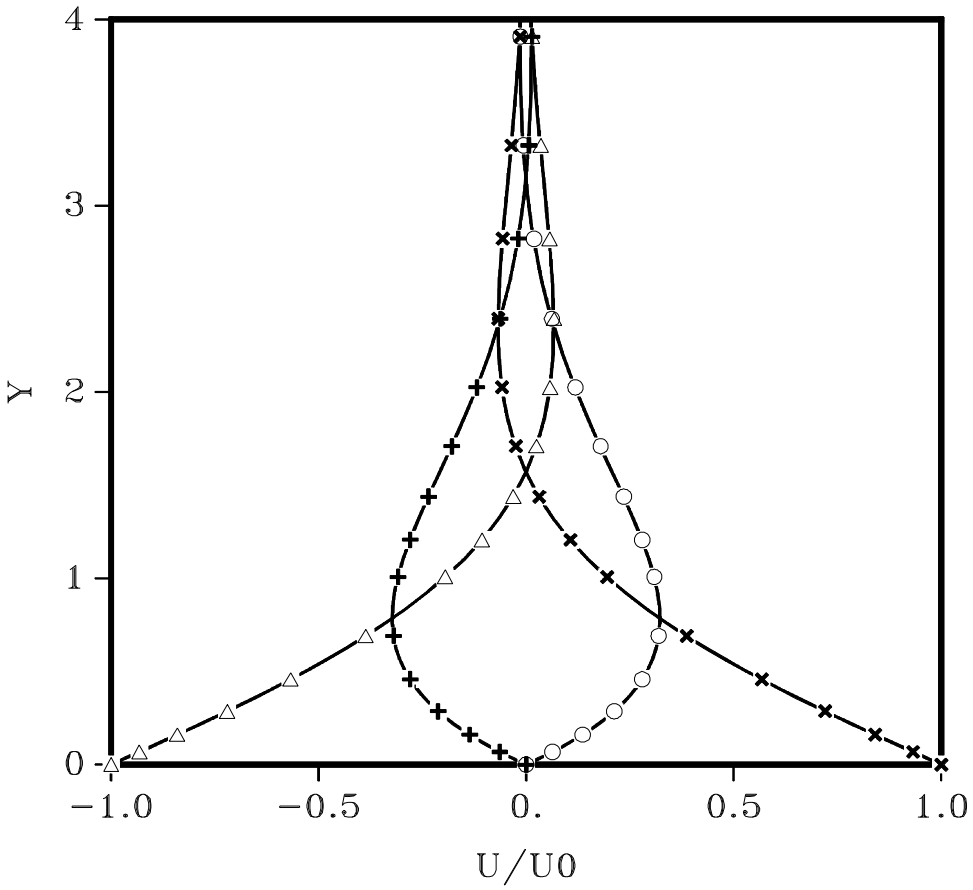

Fig. 1 Velocity profiles for flow over an oscillating plate. Solid line: computed solution; Symbols: analytical solution; ○: t=8.25; △: t=8.5; +: t=8.75; ×: t=9.

One Dimensional Channel

The flow through an inviscid 1-D channel with an oscillating back pressure was calculated. This problem was also used by Merkle and Athavale[5] to verify their method. The present work used the 2-D code by setting all gradients in the y-direction to zero and using an equally spaced grid of 21 points in the x-direction. At the inflow, constant total pressure was specified, and the static pressure at the outflow was set to be

$$p_{exit} = p_0 + p_e \sin\omega t$$

An exact analytical solution exists for this as long as the magnitude of the back-pressure oscillation p_e remains small compared to the mean back pressure p_0. For this problem, the ratio of p_e to p_0 is taken to be 0.1. The flow was calculated for a channel length of unity and a mean velocity of unity. In this case the solution is given by

$$\begin{aligned} u(t) &= 1 - \frac{p_e}{1+\omega^2}\left(\sin\omega t - \omega\cos\omega t - \omega e^{-t}\right) \\ p(x,t) &= p_0 + p_e \sin\omega t \\ &+ (x-1)\frac{p_e\omega}{1+\omega^2}\left(\cos\omega t + \omega\sin\omega t + e^{-t}\right) \end{aligned} \tag{31}$$

Both the pressure and velocity have exponentially decaying terms corresponding to the initial transient, as well as the periodic sine and cosine terms. The velocity is a function of time only, which is a direct effect of the incompressible continuity condition in a constant area duct.

The initial conditions for the problem were taken to be the velocity and pressure given by Eq. (31) evaluated at t=0. The problem was calculated for six different frequencies ranging from 0.01 to 100.0. The physical time step was taken so that 30 steps would be used for one period of the back-pressure oscillations. Thus

$$\Delta t = \frac{\pi}{15\omega}$$

The artificial compressibility constant β was set to 10 and the pseudo-time step $\Delta\tau$ was set to $10.^{12}$ Each sub-iteration in pseudo-time was converged until the maximum divergence of velocity at any point was less than 10^{-6} and the maximum element of the right-hand side of Eq. (7) was less than $10.^{-6}$ This required five to eight subiterations to obtain this convergence for all cases calculated.

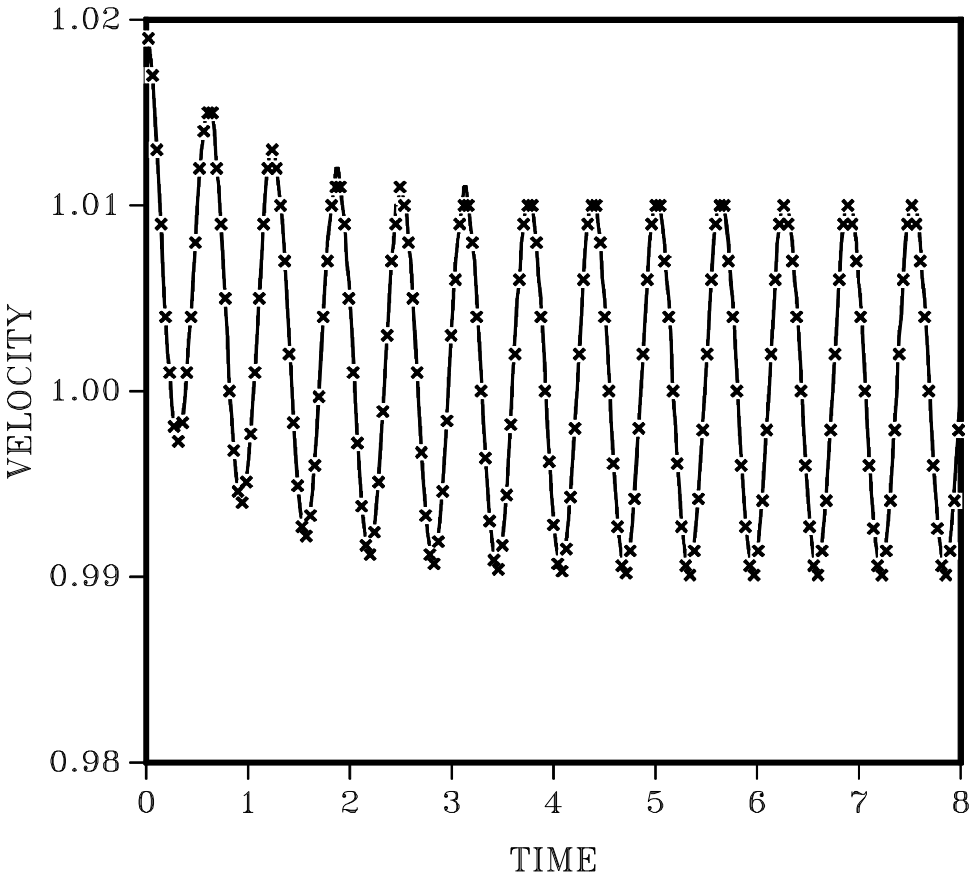

Fig. 2 Velocity for the flow through an inviscid channel with oscillating back pressure. Solid line: computed solution; ×: analytical solution.

The velocity is plotted as a function of time in Fig. 2. Shown are the computed values (solid line), and the exact values ($\times$ symbol) for a frequency of $\omega = 10$. The transient is seen to die out after about five periods, after which simple harmonic motion occurs. The results compare very well with each other, except that the computed mean velocity for the periodic motion is equal to 1.00035, whereas the exact mean velocity is 1. The values of the computed pressure are seen

to be quite accurate as well. The maximum error of the computed pressure was measured for all cases run and was found to average less than $10,^{-4}$ which corresponds to an error of about 0.01 percent.

Circular Cylinder

The flow over a circular cylinder was computed in an effort to induce vortex shedding in the wake. Computations were carried out at two different Reynolds numbers of 105 and 200.

Reynolds number 200

The Reynolds number 200 case was run first and quantitative measurements of the flow field were taken. This case was run using a 60 by 100 O-grid with points clustered near the body such that the spacing next to the surface was 0.0035 diameters. The outer boundary extended to 10 diameters from the cylinder, a physical time step Δt of 0.025 was used, and the artificial compressibility constant β was set to 2500. Both the fifth- and third-order accurate convective flux differences were used.

At each time step the subiterations were carried out until both the maximum divergence of velocity at any point and the maximum residual at any point was less than 10^{-4}. During the initial transient, 20 to 30 subiterations were required for each time step, but this quickly decreased to an average of 5 subiterations per time step. Once an asymmetric wake developed, 12 to 14 subiterations were required.

The flow was started impulsively from free-stream conditions and run until a periodic shedding of vortices occurred. The vortex shedding developed without any type of artificial disturbance. This is most probably due to the roundoff error adding some very small asymmetric disturbances which will trigger the asymmetric motion. However, the fifth-order calculations started to develop an asymmetric wake within a nondimensional time of 50 and was completely periodic by a time of 100, whereas the additional dissipation of the third-order scheme delayed the formation of a completely periodic solution until a nondimensional time of 180.

The lift and drag coefficients for the fifth-order calculations are plotted versus time in Fig. 3. The time history for the third-order calculations is quite similar to this plot. However the quantitative results do vary. This is shown in Table 1 where the values of the lift and drag coefficients for the periodic state are listed, as well as the Strouhal number. Also listed in this table are the results from several other calculations by Rosenfeld,[15] Lecointe and Piquet,[16] Martinez,[17] Lin *et al.*,[18] and Thoman and Szewczyk.[19] Experimental results of Wille,[20] Kovasznay,[21] and Roshko[22] are included as well. A wide range of values exist for these parameters. Values for the Strouhal number near 0.19 appear to be quite consistent, and so the Strouhal number of the present result for the third-order differencing appears to be too low. The difference between the third- and fifth-order schemes could be attributed to the difference in the amount of numerical dissipation which is added by each scheme.

In Fig. 4, the streamlines at various stages during one period are plotted for the third-order calculations. The first plot shows the flow when the drag is at a minimum and the lift is zero. It can be seen that a new vortex is forming on the top half, while the low-pressure center of the previous vortex has pulled away from the body causing the drop in drag. The second plot shows that the top vortex has now extended itself across the entire back side of the body, causing this point in time to have a maximum in drag and lift. The next two plots correspond to another minimum in drag with zero lift, and a maximum in drag with a minimum in lift, respectively. These two are mirror images of the first two plots. Finally, the last plot is nearly identical to the first one, and is only different because it is taken at a time of 6 after the first plot, whereas the actual period for this flow is 6.25. The main qualitative flow features shown here are the same as are seen in the fifth-order calculations.

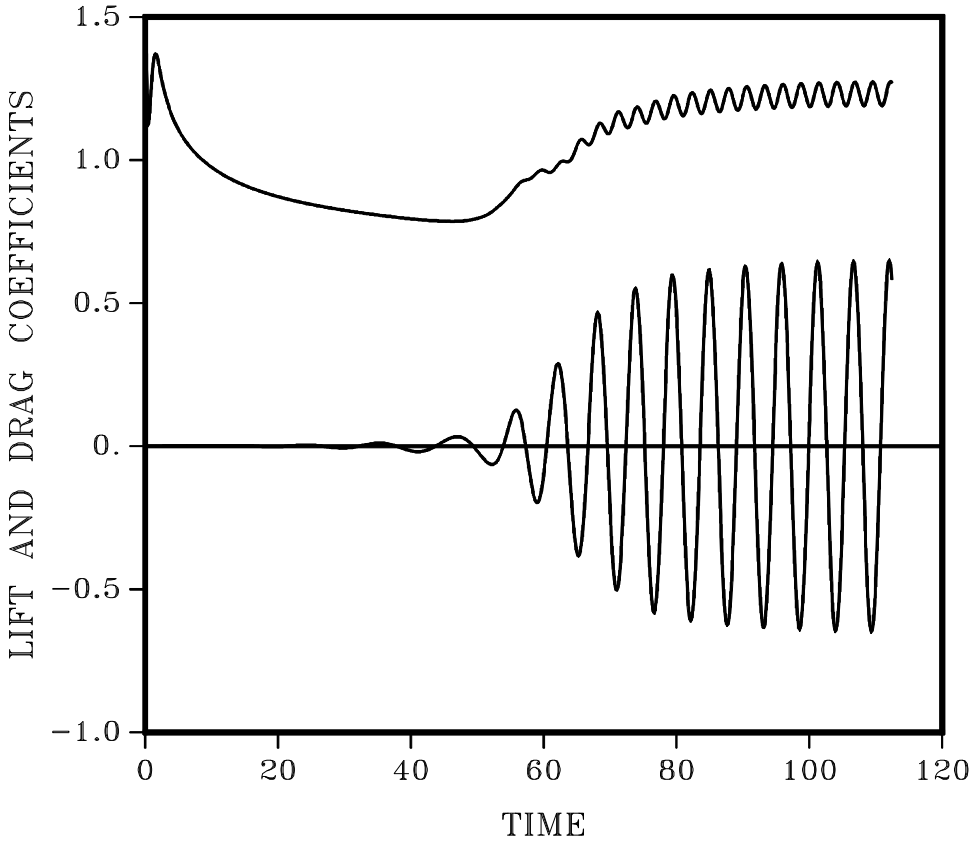

Fig. 3 Lift and drag coefficients versus time for flow over a circular cylinder at a Reynolds number of 200.

Table 1 Lift and drag coefficients and strouhal numbers for circular cylinder flow at reynolds number 200

	C_D	C_L	St
Present 3rd order	1.29 ± 0.05	± 0.75	0.16
Present 5th order	1.23 ± 0.05	± 0.65	0.185
Rosenfeld[15]	1.46 ± 0.05	± 0.69	0.211
Lecointe & Piquet[16]			
2nd order	1.46 ± 0.04	± 0.70	0.227
4th order	1.58 ± 0.0035	± 0.50	0.194
Martinez[17]	1.27 ± 0.0035		
Lin *et al.*[18]	1.17		
Thoman & Szewczyk[19]	1.17 ± 0.005		
Wille[20] (exp)	1.3		
Kovasznay[21] (exp)			0.19
Roshko[22] (exp)			0.19

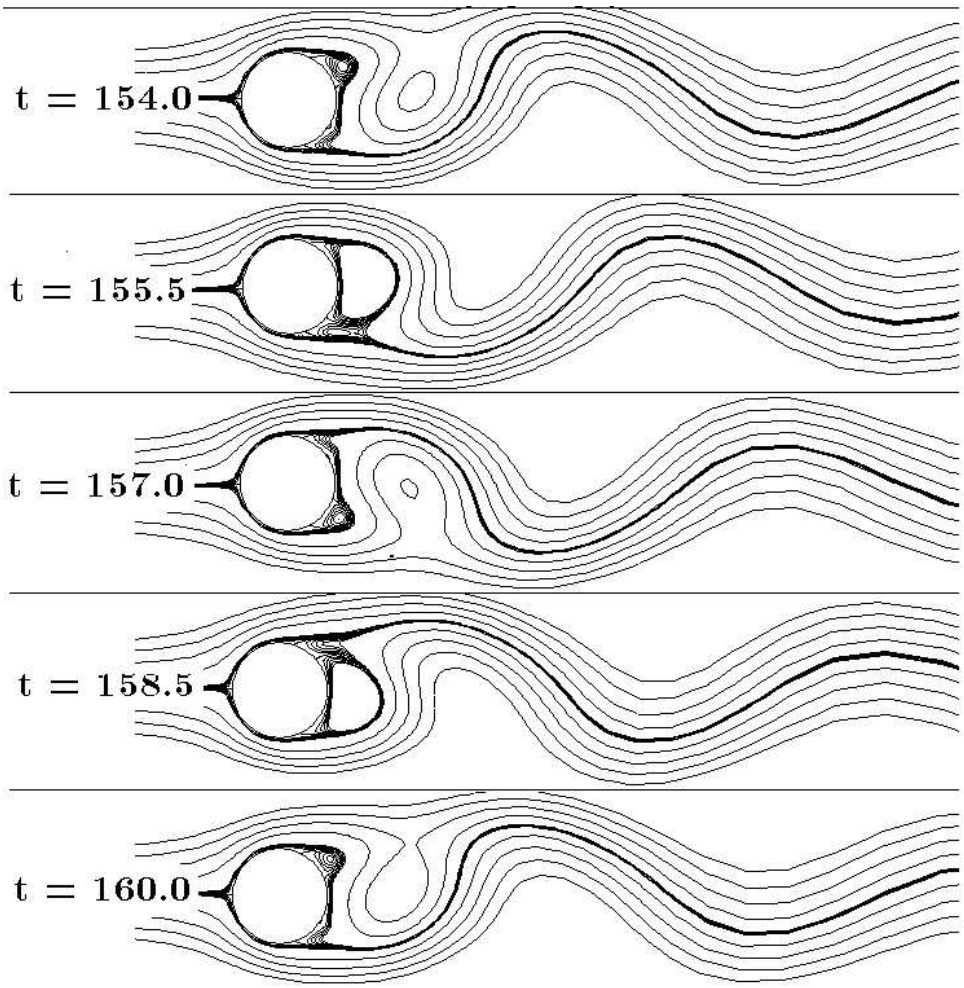

Fig. 4 Streamlines for flow over a circular cylinder at a Reynolds number of 200 at various times during the vortex shedding cycle for the third-order differencing scheme.

Reynolds number 105

The code was next run for a circular cylinder at a Reynolds number of 105 in an effort to see how well the Kármán vortex street is captured by the upwind differencing scheme. The grid dimensions were increased to 120 by 240 points in the radial and circumferential directions, respectively, and the outer boundary was extended to 25 diameters away from the cylinder. A physical time step of 0.05 was used, and the value of β was set to 1100. The fifth-order convective flux differences were used. In order to reduce the computing time required to see the vortex shedding, an artificial velocity disturbance along one side of the cylinder was added. The surface velocity on one side was prescribed to be sinusoidal in time with a non-dimensional frequency of 0.16 and a magnitude of one quarter of the freestream velocity. This triggered shedding right away, and the disturbance was turned off after a non-dimensional time of 15.7, after which time the vortex shedding continued and a completely periodic solution was obtained within several cycles. With this finer grid, an average of 30 subiterations were required at each time step.

Streaklines were computed for this periodic solution at a non-dimensional time of 58 and are shown in Fig. 5a. Below this is Fig. 5b, an experimental picture of the same flow conditions by Sadatoshi Taneda reproduced from Van Dyke[23]. The streaklines in the experiment are shown by electrolytic precipitation in water. The vortex structure is seen to be very similar between the two.

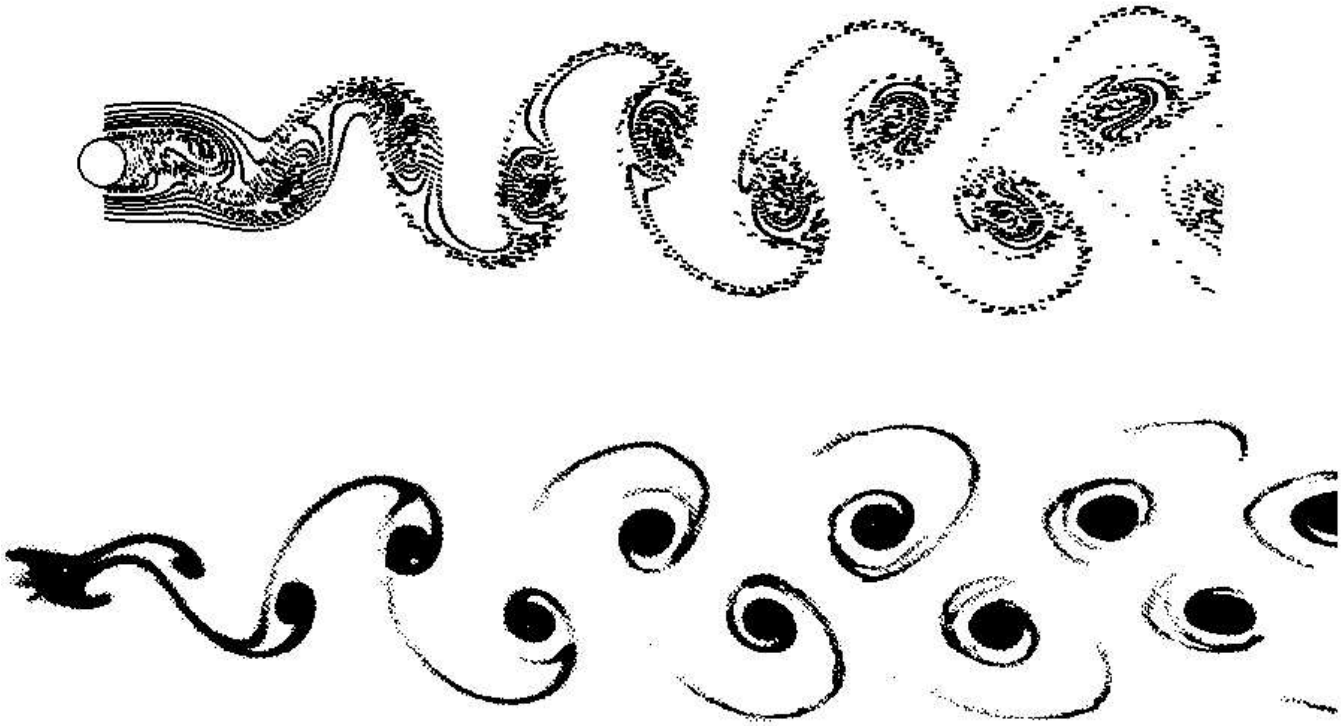

Fig. 5 Comparison between computational and experimental streaklines for the flow over a circular cylinder at a Reynolds number of 105.

Airfoil at -90 Degrees Angle of Attack

The flow of the wake of a lifting rotor over the wing of the XV-15 Tilt Rotor aircraft will degrade the lifting capability of the aircraft in hover. The vertical drag thus created can cause a penalty of 5 to 15 % of the gross weight of the aircraft.[24] Although the flow over such a configuration is largely 3-D, some useful information about this phenomenon may be obtained by studying the flow over a 2-D airfoil at -90 degrees angle of attack. The current code was used to perform such a calculation over an NACA 64A223M airfoil. A 53 by 101 O-grid was generated using the hyperbolic grid generation method of Cordova and Barth.[25] The spacing next the to airfoil was 10^{-3} chord lengths, and the outer boundary extends to 7 chords away from the airfoil. Figure 6 shows the near-field region of this grid. The physical time step Δt was set to 0.025 and the time step in pseudo-time was set to 10.[12] The fifth-order scheme was used for the upwind-differenced fluxes, and the artificial compressibility constant β was set to 2200. The number of sub-iterations required at each time step varied between 15 and 20 during the course of the computation.

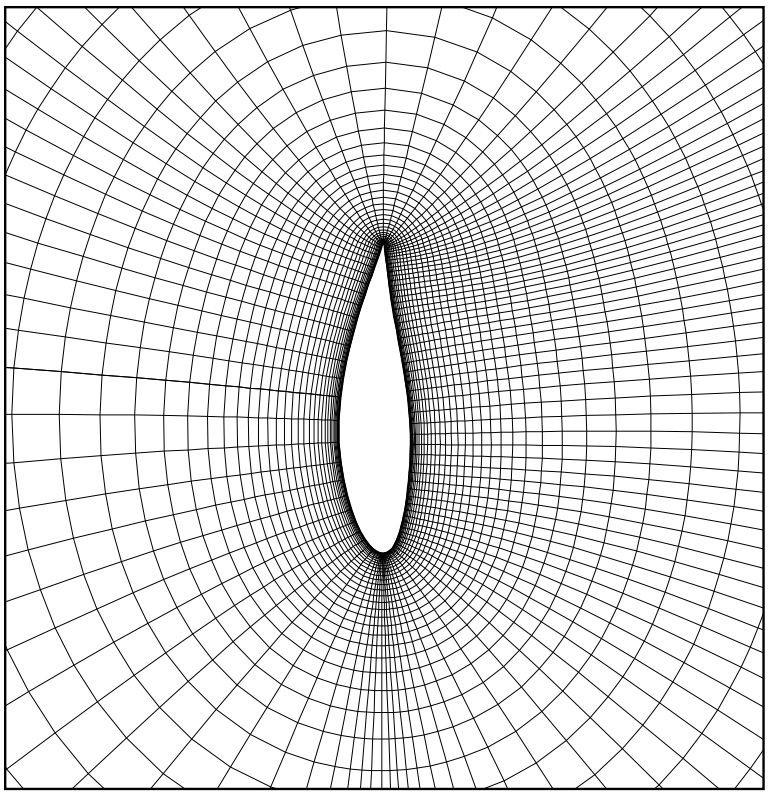

Fig. 6 Grid used in the computation of flow over an NACA 64A223M airfoil and -90 degrees angle of attack.

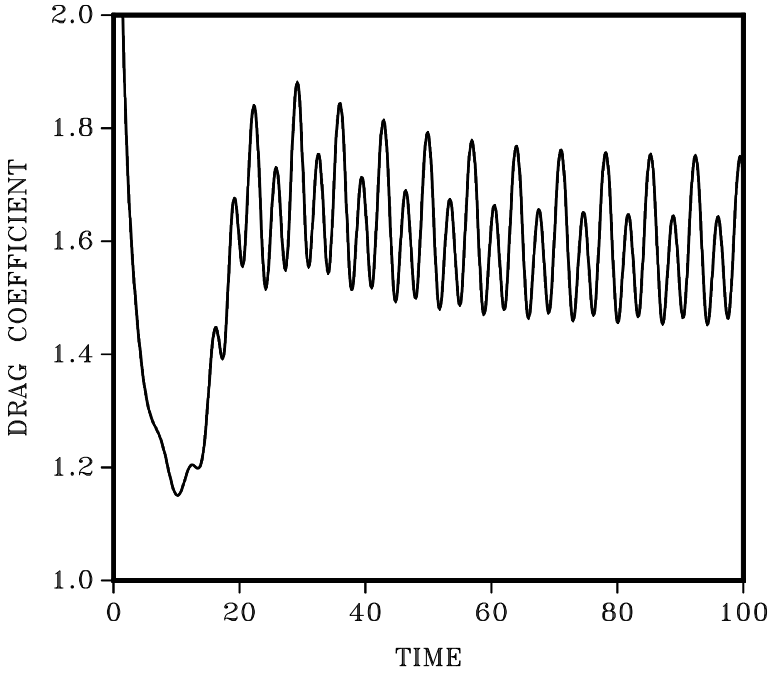

Fig. 7 Coefficient of drag versus time for the flow over an airfoil at -90 degrees of attack and a Reynolds number of 200.

The time history of the drag coefficient is plotted in Fig. 7. This shows that the flow entered into a periodic shedding cycle a short time after the start from freestream conditions. The curve shows that the drag coefficient has two separate maximum at alternate cycles. This is easily understood by examining streamlines shown in Fig. 8. In the first of these plots the low pressure core of the fully developed vortex has pulled away approximately one chord from the body, causing the drag to be at a minimum. The next vortex which forms at the trailing edge is fully developed in the next plot, and the drag is at is largest maximum. In the next two plots, the trailing edge vortex pulls off the body, first causing a minimum in drag, and then the leading edge vortex becomes fully developed, causing the smaller of the two drag maximum. The last plot completes the period and is seen to be identical to the first set of streamlines.

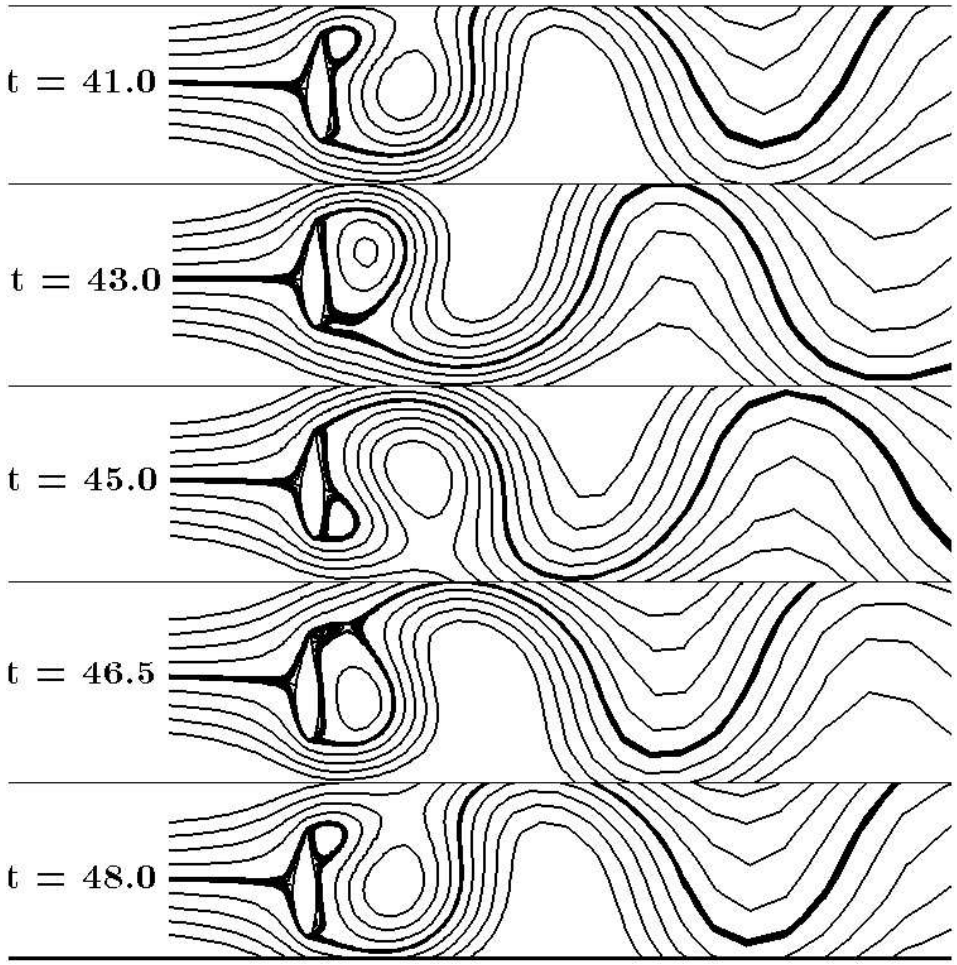

Fig. 8 Streamlines of flow over an airfoil at -90 degrees angle of attack and a Reynolds number of 200 for various times during the vortex shedding cycle.

Conclusions

The method of artificial compressibility has afforded a direct coupling between velocity and pressure, requiring the convergence of a hyperbolic system of equations to advance the variables in physical time. Since the system of equations is hyperbolic, upwind differencing based on

flux-difference splitting can be used to provide highly accurate, smooth solutions. The use of an implicit line-relaxation scheme provides the means by which the system can be advanced in physical time using a fairly small number of sub-iterations. Implicit, nonreflective boundary conditions based on the method of characteristics have been developed, and allow the placement of the boundary to be relatively close to the body. The time-accurate scheme has been verified with several computations ranging from very simple flows, where the computations agreed well with the known analytical solutions, to the more complex flows involving vortex shedding, where successful comparison between experimental data and other computational data was made.

It is thought that if an optimum β can be found, the sub-iteration convergence can be improved, leading to an efficient solution method which can be extend to large 3-D problems. A stability analysis of the system may help in setting guidelines for the choice of the optimum β. In addition, further work needs to be done to determine how the accuracy is affected by the order of the convergence during the sub-iteration cycle at every time step.

Acknowledgements

This work was partially sponsored by NASA Marshall Space Flight Center.

References

[1] Harlow, F. H. and Welch, J. E., "Numerical Calculation of Time-Dependent Viscous Incompressible Flow with Free Surface," *Physics of Fluids*, Vol. 8, Dec. 1965, pp. 2182–2189.

[2] Chorin, A. J., "Numerical Solution of the Navier-Stokes Equations," *Math. Comp.*, Vol. 22, 1968, pp. 745–762.

[3] Chorin, A. J., "A Numerical Method for Solving Incompressible Viscous Flow Problems," *J. Comp. Phys.*, Vol. 2, 1967, pp. 12–26.

[4] Kwak, D., Chang, J. L. C., Shanks, S. P., and Chakravarthy, S. R., "A Three-Dimensional Incompressible Navier-Stokes Flow Solver Using Primitive Variables," *AIAA J.*, Vol. 24, 1986, pp. 390–396.

[5] Merkle, C. L. and Athavale, M., "Time-Accurate Unsteady Incompressible Flow Algorithms Based on Artificial Compressibility," AIAA Paper 87-1137, 1987.

[6] Soh, W. Y. and Goodrich, J. W., "Unsteady Solution of Incompressible Navier-Stokes Equations," To be published in *J. Comp. Phys.*

[7] Rogers, S. E. and Kwak, D., "An Upwind Differencing Scheme for the Steady-State Incompressible Navier-Stokes Equations," NASA TM 101051, Nov. 1988.

[8] Hartwich, P. M. and Hsu, C. H., "High Resolution Upwind Schemes for the Three-Dimensional Incompressible Navier-Stokes Equations," AIAA Paper 87-0547, 1987.

[9] Rogers, S. E., Chang, J. L. C., and Kwak, D., "A Diagonal Algorithm for the Method of Pseudocompressibility," *J. Comp. Phys.*, Vol. 73, No. 2, 1987, pp. 364–379.

[10] Rai, M. M., "Navier-Stokes Simulations of Blade-Vortex Interaction Using High-Order Accurate Upwind Schemes," AIAA Paper 87-0543, 1987.

[11] Barth, T. J., "Analysis of Implicit Local Linearization Techniques for Upwind and TVD Algorithms," AIAA Paper 87-0595, 1987.

[12] Yee, H. C., "Linearized Form of Implicit TVD Schemes For The Multidimensional Euler and Navier-Stokes Equations," *Comp. and Maths. with Appls.*, Vol. 12A, Nos. 4/5, 1986, pp. 413–432.

[13] Merkle, C. L. and Tsai, P. Y. L., "Application of Runge-Kutta Schemes to Incompressible Flow," AIAA Paper 86-0553, 1986.

[14] White, F. M., *Viscous Fluid Flow*, McGraw-Hill, New York, 1974, pp. 148–149.

[15] Rosenfeld, M., Kwak, D., and Vinokur, M., "A Solution Method for the Unsteady and Incompressible Navier-Stokes Equations in Generalized Coordinate Systems," AIAA Paper 88-0718, 1988.

[16] Lecointe, Y. and Piquet, J., "On the Use of Several Compact Methods for the Study of Unsteady Incompressible Viscous Flow Round a Circular Cylinder," *Computers & Fluids*, Vol. 12, No. 4, 1984, pp. 255–280.

[17] Martinez, G., "Caractéristiques Dynamiques et Thermiques de l'Écoulements Autour d'un Cylindre Circulaire à Nombres de Reynolds Modérés," *Thèse D. I. – I. N. P. Toulouse*, 1979.

[18] Lin, C. L., Pepper, D. W., and Lee, S. C., "Numerical Methods for Separated Flow Solutions Around a Circular Cylinder," *AIAA J.*, Vol. 14, 1976, pp. 900–907.

[19] Thoman, D. and Szewczyk, A., "Time Dependent Viscous Flow Over a Circular Cylinder," *Phys. Fluids, suppl. II*, 1969, pp. 79–86.

[20] Wille, R., "Karman Vortex Streets," *Adv. Appl. Mech.*, Vol. 6, 1960, pp. 273.

[21] Kovasznay, L. S. G., "Hot-wire Investigation of the Wake Behind Cylinders at Low Reynolds Numbers," *Proc. Roy. Soc. A*, Vol. 198, 1949, pp. 174–190.

[22] Roshko, A., "On the Development of Turbulent Wakes From Vortex Streets," NACA Rep. 1191, 1954.

[23] Van Dyke, M., *An Album of Fluid Motion*, The Parabolic Press, Stanford, California, 1982, p. 57.

[24] McCroskey, W. J., Spalart, Ph., Laub, G. H., Maisel, M. D., and Maskew, B., "Airloads on Bluff Bodies, with Application to the Rotor-Induced Downloads on Tilt-Rotor Aircraft, " *Vertica*, Vol. 9, No. 1., 1985, pp. 1–11.

[25] Cordova, J. Q., and Barth, T. J., "Grid Generation For General 2-D Regions Using Hyperbolic Equations," AIAA Paper 88-0520, 1988.